JACS
JOURNAL OF THE AMERICAN CHEMICAL SOCIETY
Article
pubs.acs.org/JACS

Energetic Salts with π-Stacking and Hydrogen-Bonding Interactions Lead the Way to Future Energetic Materials

Jiaheng Zhang,[†] Qinghua Zhang,[†,‡] Thao T. Vo,[†,§] Damon A. Parrish,[∥] and Jean'ne M. Shreeve*[,†]

[†]Department of Chemistry, University of Idaho, Moscow, Idaho 83844-2343, United States
[‡]Institute of Chemical Materials, China Academy of Engineering Physics, Mianyang 621900, China
[§]Indian Head Explosive Ordnance Disposal Technology Division, The Naval Surface Warfare Center, Indian Head, Maryland 20640, United States
[∥]Naval Research Laboratory, 4555 Overlook Avenue, Washington, D.C. 20375, United States

Supporting Information

ABSTRACT: Among energetic materials, there are two significant challenges facing researchers: 1) to develop ionic CHNO explosives with higher densities than their parent nonionic molecules and (2) to achieve a fine balance between high detonation performance and low sensitivity. We report a surprising energetic salt, hydroxylammonium 3-dinitromethanide-1,2,4-triazolone, that exhibits exceptional properties, viz., higher density, superior detonation performance, and improved thermal, impact, and friction stabilities, then those of its precursor, 3-dinitromethyl-1,2,4-triazolone. The solid-state structure features of the new energetic salt were investigated with X-ray diffraction which showed π-stacking and hydrogen-bonding interactions that contribute to closer packing and higher density. According to the experimental results and theoretical analysis, the newly designed energetic salt also gives rise to a workable compromise in high detonation properties and desirable stabilities. These findings will enhance the future prospects for rational energetic materials design and commence a new chapter in this field.

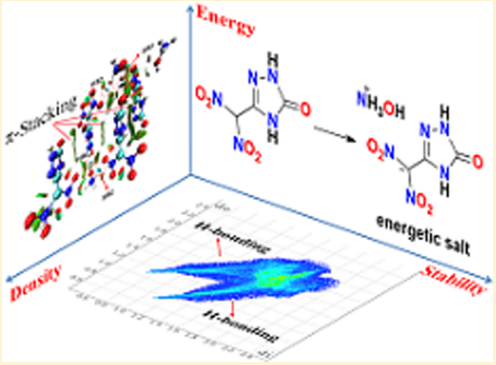

INTRODUCTION

More than a century has passed since Alfred Nobel refined the process for manufacturing dynamite; however, although Nobel's legacy still lives on, current explosives are totally different. Throughout the development history of energetic materials, it can be outlined from the discovery of gunpowder, formulation for explosives, and currently, molecular design for high performance.[1,2] Each succeeding generation has significantly enhanced the capability of energetic materials by improving performance and/or safety.[3,4] Modern explosives as well as propellants are required to be high energy density materials (HEDMs) that can release tremendous energy on demand.[4] The desirable characteristics for these materials include high detonation velocity and pressure, high density, good thermal stability, good environmental compatibility, and low sensitivity toward impact and friction.[5,6] However, achieving a fine balance between high detonation performance and low sensitivity is often a huge challenge since the enhanced properties come mostly at the expense of molecular stability.[7] Therefore, the leading innovations of the next-generation of HEDMs are not only in pursuit of novel molecular design but also focus on a combination of physics, crystallography, and chemistry to prepare high-level energy sources.[8−10]

In addition to energetic cocrystals and energetic metal organic frameworks, another powerful and straightforward route to next-generation HEDMs is through the formation of energetic salts.[11−13] In essence, this approach expands the utility of common acidic polynitro-substituted heterocycles by including a larger series of related salts. The salts share major parts of their parent molecules, and thus their inherent individual properties, yet their behaviors differ because of cation−anion interactions as well as distinct crystal packing.[14] Of all well-known energetic cations, the hydroxylammonium cation outshines the competition because of its obvious advantages such as high nitrogen and oxygen percentages, high heat of formation, simple preparation and purification, and low cost.[15,16] During the past decade, we have concentrated our efforts on the design and development of novel energetic salts and have often found that hydroxylammonium energetic salts possess better detonation performances and stabilities than their precursors.[16−18] Some outstanding examples of this salt-type exhibit excellent properties and are even superior to those of typical HEDMs, such as 1,3,5-trinitroperhydro-1,3,5-triazine (RDX), and octahydro-1,3,5,7-tetranitro-1,3,5,7-tetrazocine (HMX).[13] In particular, an important representative, hydroxylammonium nitrate, which was developed by a U.S. Air Force Research Laboratory and applied as a high-performance green

Received: December 17, 2014
Published: January 7, 2015

DOI: 10.1021/ja5126275
J. Am. Chem. Soc. 2015, 137, 1697−1704

Scheme 1. Synthesis of 1 and 2

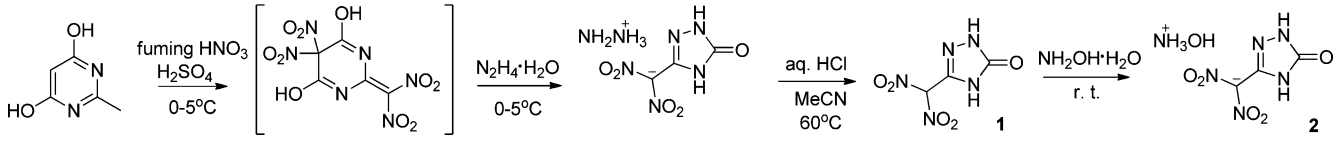

propellant, has already highlighted the potential of these high-energy salts for application.[19]

One of the remaining significant challenges in this field is the creation of ionic CHNO energetics with higher densities than their precursors. This appears fairly simple for metal salts where the bonding is delocalized, nondirectional, and "soft", so that the close packing which maximizes nondirectional cation−anion interactions usually leads to higher density.[20,21] However, when the formation of the organic anion and nonmetal cation is taking place, driving forces are directional cation−anion interactions along with weak interactions.[22,23] Therefore, the formation of CHNO salts usually results in an average density falling between the parent compounds. To the best of our knowledge, there are rare energetic ionic CHNO compounds, particularly no known hydroxylammonium salt, which are more dense than their precursors. In this respect, the notion of "high-density energetic salt" is essentially unfulfilled.

In this study, we report the first hydroxylammonium salt, hydroxylammonium 3-dinitromethanide-1,2,4-triazolone, that is more dense than the parent nonionic compound. Importantly, due to the distinct factors of the ionic form such as high nitrogen content, higher density, and higher heat of formation, the newly designed energetic salt also exhibits superiority in all aspects of detonation properties over its precursor. Furthermore, a detailed investigation based on structure factors by X-ray diffraction indicated the importance of weak interactions especially $\pi-\pi$ interactions and hydrogen-bonds in closer packing. Another interesting point is that these structural features can also contribute to enhanced thermal, impact, and friction stabilities based on experimental and theoretical analysis. In view of these findings, it was desirable to design energetic salts with π-stacking and hydrogen-bonding interactions as the next-generation high energy density materials in the following research.

RESULTS AND DISCUSSION

Synthesis and Crystal Structures. First, the intermediate product hydrazinium 3-dinitromethanide-1,2,4-triazolone was prepared according to a modified procedure by treating the nitration product of 4,6-dihydroxy-2-methylpyrimidine with hydrazine hydrate at 0 °C.[24] Then, 3-dinitromethyl-1,2,4-triazolone (**1**) was obtained by neutralizing the hydrazinium 3-dinitromethanide-1,2,4-triazolone with concentrated HCl in an acetonitrile solution. The corresponding hydroxylammonium salt (**2**) was synthesized in a straightforward manner by an acid−base reaction using 50% hydroxylamine solution (Scheme 1).

Characterization of these compounds was accomplished through infrared and multinuclear NMR spectroscopy and elemental analysis. Both of the compounds which were synthesized are nonhygroscopic and stable in air. Crystals of **1** and **2**, suitable for single-crystal X-ray diffraction, were obtained by slow evaporation of water solutions at room temperature. The X-ray crystal structures confirmed that the dinitromethyl group of **1** (Figure 1a) was deprotonated to form the monosalt **2** (Figure 1b).

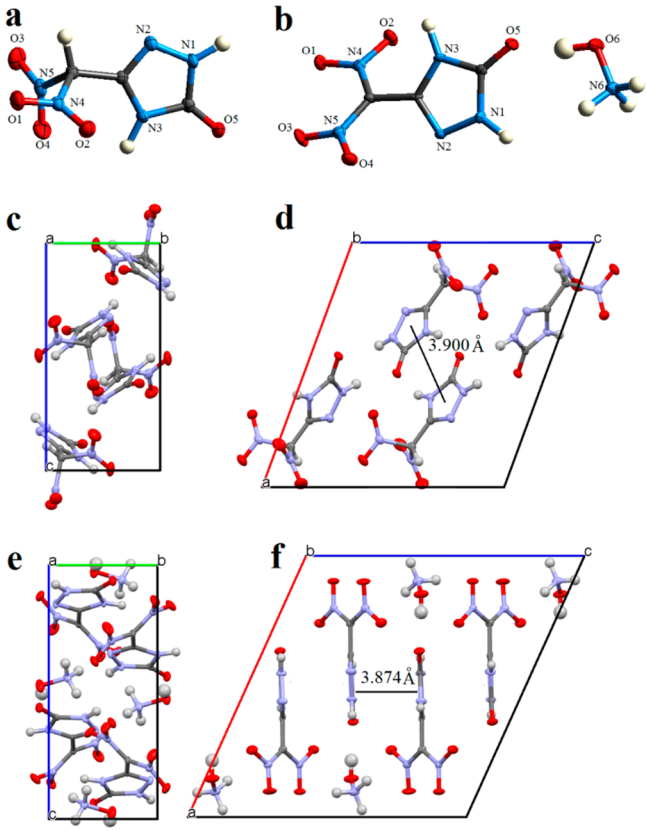

Figure 1. Single-crystal X-ray structures of **1** (a) and hydroxylammonium **2** (b), with thermal ellipsoids drawn at the 50% probability level, produced using CrystalExplorer software.[25] View of **1** along the (c) *a* axis and (d) *b* axis. View of **2** along the (e) *a* axis and (f) *b* axis.

Density of Energetic Materials. Density is one of the most important physical properties of energetic materials. A density value >1.80 g cm^{-3} is an essential requirement for advanced energetic materials.[2] With respect to **1** and **2**, the crystal densities are observed to be 1.922 and 1.929 g cm^{-3} calculated at 150 and 173 K, respectively. The packing coefficient is measured as the ratio of total molecular volume to unit cell volume where 0.79 for **2** is higher than that of **1** (0.77). The densities based on gas-pycnometer measurements of the anhydrous compounds at 25 °C are 1.906 and 1.910 g cm^3 for **1** and **2**, which outperform most currently used energetics and are comparable with that of HMX (1.91 g cm^{-3}).

Remarkably, it is unexpected that the density of the salt would be higher than that of the precursor. Since this observation appeared to be different from the usual case, we were encouraged to search for a rationale. The density of energetic materials is a result of molecular packing. Since it would be expected that **1** and **2** would exhibit different behaviors in crystal stacking,[26] the unit cell packing for each

DOI: 10.1021/ja5126275
J. Am. Chem. Soc. 2015, 137, 1697−1704

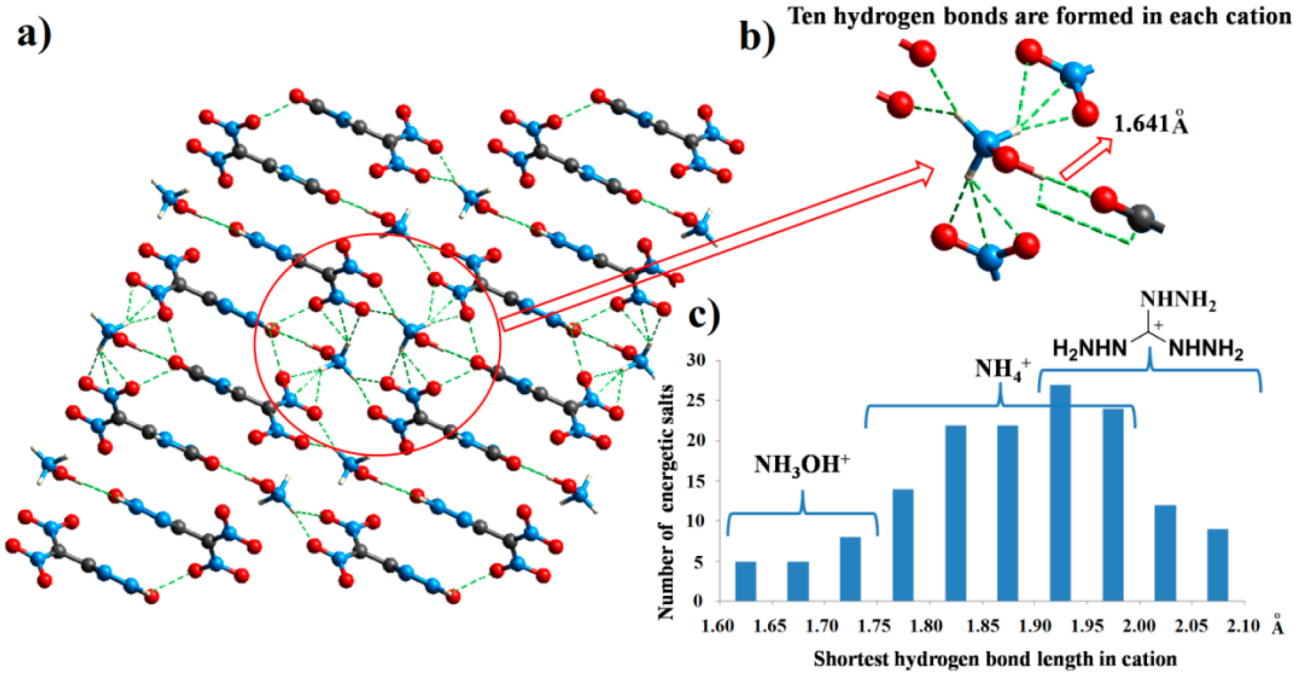

Figure 2. Hydrogen-bonding interaction analysis. (a) The hydrogen-bond network of **2**; (b) Ten intramolecular and intermolecular hydrogen-bonds in the hydroxylammonium cation were observed; (c) The shortest hydrogen···acceptor distribution between cation hydrogens and hydrogen bond acceptor for various energetic salts (150 hits from Cambridge Structural Database).

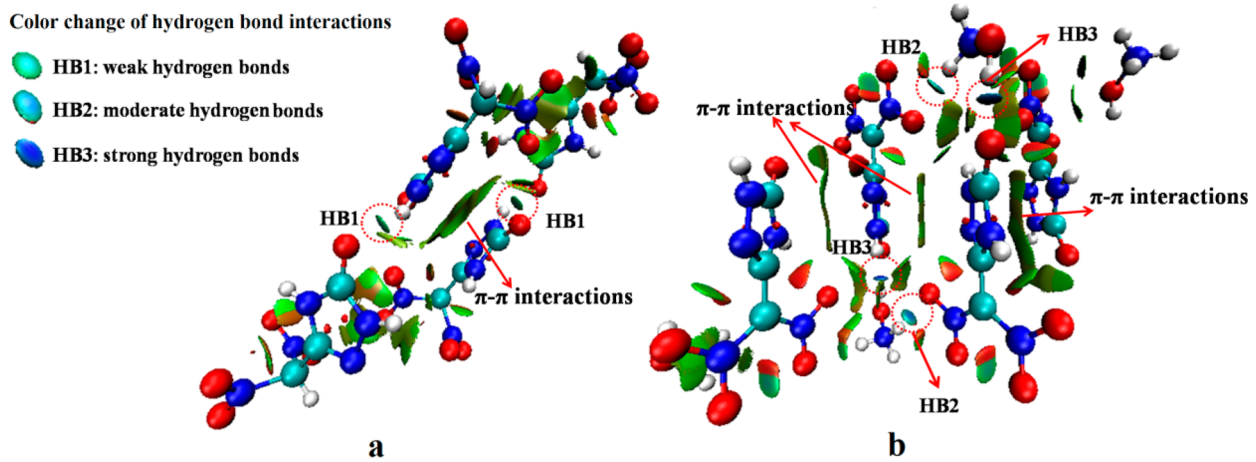

Figure 3. NIC plots of gradient isosurfaces (s = 0.5 au) for 1 (a) and 2 (b) unit cells. The geometries of the unit cells were optimized at the BLYP-D3/def2-QZVPP method[32] using ORCA 3.0.[33] The surfaces are colored on a blue-green-red scale indicating strong attractive interactions, weak attractive, and strong nonbonded overlap, respectively.

crystal was examined. As shown in Figure 1c,d, two of the 3-dinitromethyl-1,2,4-triazolone molecules are in a parallel face-to-face $\pi-\pi$ interaction and each side stacked with another molecule to form an edge-to-face arrangement. Such crystal units are repeated in an infinite stack which classifies the whole crystal as having mixing type stacking. With respect to **2** (Figure 1e,f), the crystal packing is dominated by an infinite face-to-face $\pi-\pi$ arrangement and raised nitro groups classifying the whole crystal to have wave-like-type stacking. To identify the tightness of the two crystal packing, the distances between triazolone centroids of **1** (3.900 Å, Figure 1d) were measured and compared to that of **2** (3.874 Å, Figure 1f), both of the distances belong to typical geometrical parameters of aromatic $\pi-\pi$ interactions (3.65−4.00 Å).[27] The shorter distances between triazolone centroids in **2** can be explained by electro density distribution after deprotonation of the dinitromethyl moiety of **2**, which involves recognizable single and double bonds rather than the completely delocalized π-systems in the triazolone ring.[27] Therefore, each molecule can stack in such a way that single bonds are sandwiched between double ones and vice versa. Such an arrangement also lowers repulsions of π-electrons, while increasing dipolar attraction and resulting in closer packing.[28]

Energetic salts consisting of azoles composed of high nitrogen and oxygen content cations and anions possess a large number of N−H and O−H bonds and exhibit extensive hydrogen bonding. Additional evidence that supports the higher density of salt **2** was obtained by examining the extra hydrogen-bond networks from the cation (Figure 2a). Based on the crystal structures, the hydroxylammonium cation of **2** (24

DOI: 10.1021/ja5126275
J. Am. Chem. Soc. 2015, 137, 1697−1704

Table 1. Calculated detonation parameters of compounds 1 and 2 using the EXPLO5 computer code

Comp.	N[a] [%]	N+O[b] [%]	Ω[c] [%]	d[d] [g cm^{-1}]	$\Delta_f H$[f] [kJ mol^{-1} /kJ g^{-1}]	νD[f] [m s^{-1}]	P[g] [Gpa]	I_{sp}[h] [S]
1	37.04	79.35	4	1.906	−136.6/-0.72	8597	33.1	232
2	37.84	81.06	0	1.910	−128.3/-0.58	8946	37.2	247
TNT[i]	18.50	42.26	−27	1.650	−115/-0.26	6881	19.5	211
RDX[i]	37.84	81.06	0	1.820	80.0/0.36	8748	34.9	258

[a]Nitrogen content. [b]Combined nitrogen and oxygen content. [c]Oxygen balance for $C_aH_bO_cN_d$, 1600(c-a-b/2)/M_w; M_w = molecular weight. [d] Density determined by gas pycnometer at 25 °C. [e]Calculated heat of formation. [f]Detonation velocity. [g]Detonation pressure. [h]Specific impulse. [i]Properties of TNT and RDX are taken from ref 13.

hydrogen bonds in each molecule) can provide 71% more intramolecular and intermolecular hydrogen bonds compared to **1** (14 hydrogen bonds in each molecule). Various hydrogen bonds in the cation play an important role in tightly connecting the neighboring triazolone layer (Figure 2b). In such a case, the hydrogen···acceptor (H···A) lengths of the hydrogen bonds in the hydroxylammonium cation can describe quantitatively how close the interactions between cation and anions are. Remarkably, this length of the hydrogen bond OH···O (1.641 Å) for the hydroxylammonium cation to the carbonyl of the triazolone is significantly shorter than the normal cation−hydrogen bonds for energetic materials. A Cambridge Structural Database search provided an average of 1.893 Å for the shortest H···A length for nitrogen-rich cations in 150 energetic salts.[29] The bond-length distribution is shown in Figure 2c where 1.641 Å ranks the second shortest which is next only to 1.640 Å of hydroxylammonium azidotetrazolate in our search.[30] Of interest, the shortest H···A lengths in various cations are found in specific ranges. For example, the shortest H···A lengths exhibited by the hydroxylammonium cation fall into the 1.640−1.844 Å range, while the numbers for ammonium and triaminoguanidinium cations lie between 1.772 and 1.991 and 1.924−2.147 Å, respectively (Figure 2c). This observation is also consistent with the density order of energetic salts with various cations and supports the superiority of the hydroxylammonium cation in the resulting highly dense energetic materials.

To gain more information on inter- and intramolecular effects and comprehensively study their influence on crystal packing, the noncovalent interactions (NCI) plots of **1** and **2** unit cells were calculated in real space based on electron density and its reduced gradient using the approach by Yang et al. (Figure 3).[31] In this method, analysis of the relationship between quantum-mechanical electron density (ρ) and the reduced density gradient ($s= 1/2(3\pi^2)^{1/3})|\nabla\rho|/\rho^{4/3}$) allows detection of and observation of the differences between hydrogen bonds, van der Waals interactions, and repulsive steric clashes, etc.[31] Due to the simplicity of this theory, the face-to-face $\pi-\pi$ interactions can be easily observed between parallel triazolone rings, while the NCI domains are more abundant and larger in **2** than in **1**. In comparison with face-to-face $\pi-\pi$ surface, the edge-to-face π-type interaction surfaces in **1** are smaller which indicate the limited extent of such weak interactions. The shape of hydrogen-bonding is essentially different from that corresponding to π-stacking interactions in the NCI domain; the former is characterized by the small, round shape, large accumulation of electron density. The strongest interaction, in terms of electron density at the NCI domain, is the directional cation−anion contact and directional hydrogen-bonding interaction in **2**, which can be suggested as part of the reason for closer packing.

Overall, combined with the experimental observation and theoretical analysis, the extraordinary density of salt **2** can arise from a) more regular and tighter crystal packing; b) intensive $\pi-\pi$ interactions with a closer centroid distance as well as extensive π-type interactions; and c) significantly strong hydrogen bonds in the cation and extensive hydrogen-bond interactions.

Heats of Formation for Energetic Materials. It is difficult to obtain accurate experimental values for heats of formation for energetic materials because of the inaccuracy of the calorimetric measurements. Therefore, this important property is usually evaluated using relatively high-precision theoretical methods. In this work, the geometric optimization of **1** and **2** and frequency analyses were carried out using B3LYP/6-31+G* and the single-point energies were calculated at the MP2/6-311++G** basis set.[34] Atomization energies for 1,2,4-triazolone and the hydroxylammonium cation were obtained by using G2 ab initio method.[35] The solid-state enthalpy of formation for **1** can be calculated by subtracting the heat of sublimation from the calculated gas-phase heat of formation. Employing Trouton's rule,[36] the heat of sublimation of **1** was calculating based on the decomposition temperature (See Supporting Information). For energetic salt **2**, the solid-phase heat of formation is calculated on the basis of a Born−Haber energy cycle (See Supporting Information).[37]

For **1** and **2**, the nitro and carbonyl moieties contribute a major part of the molecules and both groups have very negative heats of formation; therefore, the solid-phase heats of formation of **1** and **2** are negative and calculated to be −136.6 and −128.3 kJ mol^{-1}, respectively. However, the incorporation of a nitrogen-rich cation still can be considered a useful way to increase the heat of formation, and, in this case, it results in an increase of 8.3 kJmol^{-1} going from **1** to **2**. More importantly, by choosing a cation with a higher nitrogen content such as hydrazinium or triaminoguanidinium, the energetic salts will exhibit higher heats of formation.

Detonation Parameters for Energetic Materials. Based on the calculated heats of formation and the measured densities at ambient temperature, detonation properties of **1** and **2** were determined by EXPLO5 (v6.01) program.[38] Given the higher density and heat of formation, it is not surprising that energetic salt **2** exhibits a better performance than **1**. As can be seen in Table 1, **2** has a higher nitrogen and oxygen content than **1**. The oxygen balance is the index of the deficiency or excess of oxygen in a compound required to convert all carbon into carbon monoxide, and all hydrogen into water. In this study, **1** has an oxygen balance of 4% and that of salt **2** is 0. The oxygen balance equaling zero means complete oxidation upon detonation which results in the maximum amount of energy release. With respect to detonation velocity, the value of **1** (8597 ms^{-1}) dramatically exceeds TNT (6881 m s^{-1}) and salt **2** remarkably exceeds that value at 8946 m s^{-1}, which is higher

DOI: 10.1021/ja5126275
J. Am. Chem. Soc. 2015, 137, 1697−1704

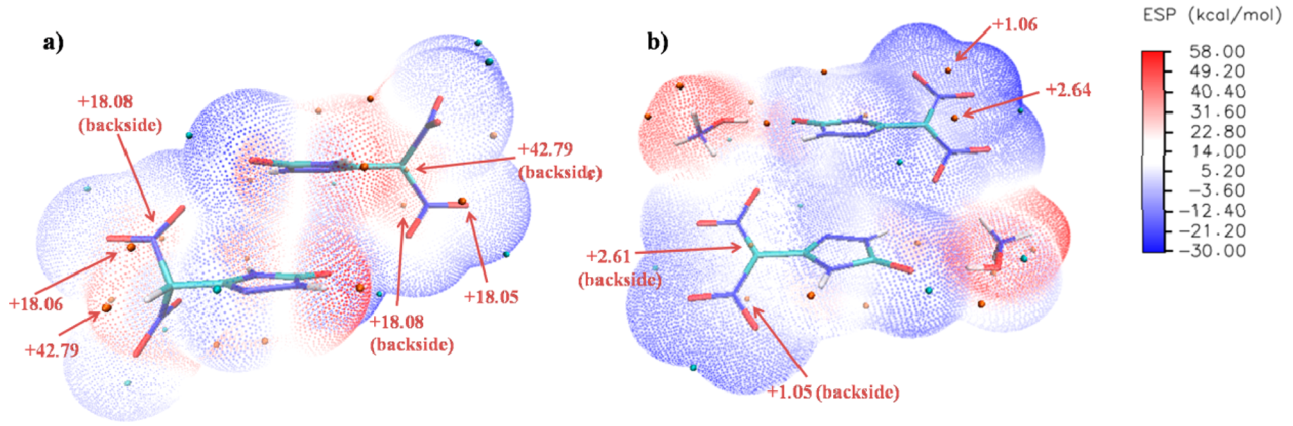

Figure 4. Electrostatic potential surfaces of **1** (**a**) and **2** (**b**). The geometries of the unit cells were optimized at the BLYP-D3/def2-QZVPP method[32] using ORCA 3.0.[33] Significant surface local minima and maxima of ESP are represented as orange and azure spheres, respectively. The maxima of ESP around C-nitro groups are labeled by brown-red texts, the units are in kcal/mol.

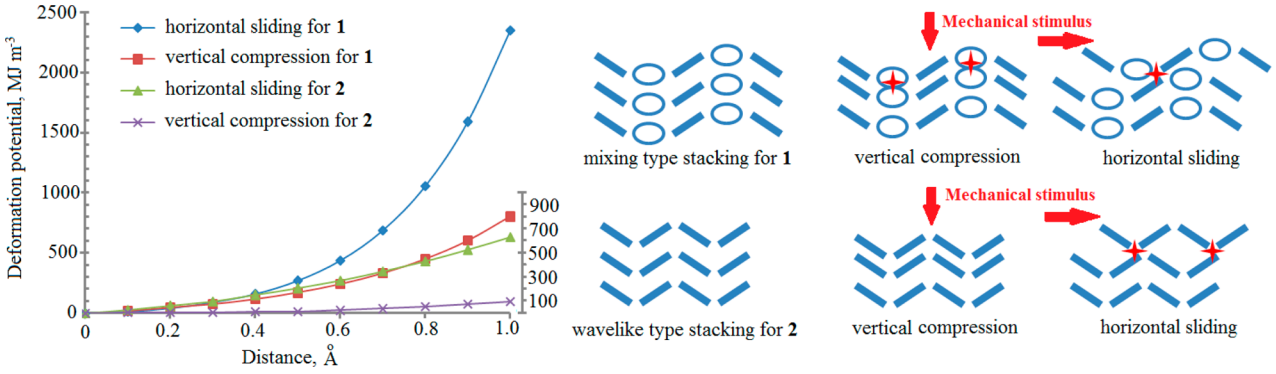

Figure 5. Deformation potential curves and horizontal sliding and vertical compression schematic diagrams of **1** and **2**. For the purpose of comparison, the central two triazolone rings in the 3-dinitromethyl-1,2,4-triazolone unit cell are placed horizontally in the calculation. Similarly, the four triazolone rings in the hydroxylammonium salt are adjusted to the horizontal position.

than RDX (8748 m s^{-1}). In terms of detonation pressures, the values for **1** (33.1 GPa) and **2** (37.2 GPa) are comparable with that of RDX (34.5 GPa). The specific impulse values, I_{sp}, for **1** and **2** were calculated as 232 and 247 s, respectively. Taken together, as long as energetic salts possess higher values for densities and heats of formation, the detonation properties will concomitantly increase, which points out the superiority of energetic salts over other types of energetic materials again.

Stabilities of Energetic Materials. Although a large set of energetic materials with excellent detonation performance have emerged recently, very few of them can practically replace current explosives or propellants. In most cases, the contradictory nature of high detonation properties and low sensitivities seriously impedes the potential application of the newly synthesized energetic materials. Among all the strategies to increase the stabilities of energetic materials, making energetic salts may be an excellent approach to maintain high-energy content with low sensitivity toward heat, impact and friction. In this study, we first demonstrated that, employing the inter- and intramolecular interactions for the construction of energetic salts can not only increase thermal stability but also lower impact and friction sensitivities.

Thermal stability is the first concern because an unacceptably low decomposition temperature will strictly limit the application of energetic materials. In this work, the phase-transition temperatures and thermal stabilities of **1** and **2** were determined by differential scanning calorimetric measurements scanning at 5 °C min^{-1}. Neither of the new compounds melts prior to decomposition; **1** has an onset decomposition temperature of 127 °C. The thermal stability of **2** greatly exceeds its parent compound with a measured onset decomposition temperature of 164 °C. Abundant studies have illustrated that bond dissociation enthalpies (BDEs) for the possible trigger bond, which is the first bond to break, is the most important factor in pyrogenic decomposition.[39] Therefore, the BDEs of **1** and **2** were calculated and the C-nitro bonds were found to be the trigger bonds for both compounds and contribute to their thermal stabilities. In agreement with experimental observation, the BDE of the C-nitro of **2** (332.3 kJ mol^{-1}) is much higher than the C-nitro BDE of **1** (182.2 kJ mol^{-1}).

Electrostatic potential surfaces (ESP) analysis for **1** and **2** dimers was carried out in order to understand the bond strength variation before and after cation−anion hydrogen bond formation.[40] It is shown clearly in Figure 4, that the C-nitro bonds of **2** are affected by these hydrogen-bonding interactions, and share the electron of hydroxylammonium cation. With regards to the electrostatic potential surfaces, after formation of hydrogen bonds, **2** possesses lower ESP values and more negative charge accumulation in the C-nitro bonds. This negative charge accumulation will shorten and strengthen the C-nitro bond, thus increasing the corresponding BDE and enhancing the thermal stability.

DOI: 10.1021/ja5126275
J. Am. Chem. Soc. 2015, 137, 1697−1704

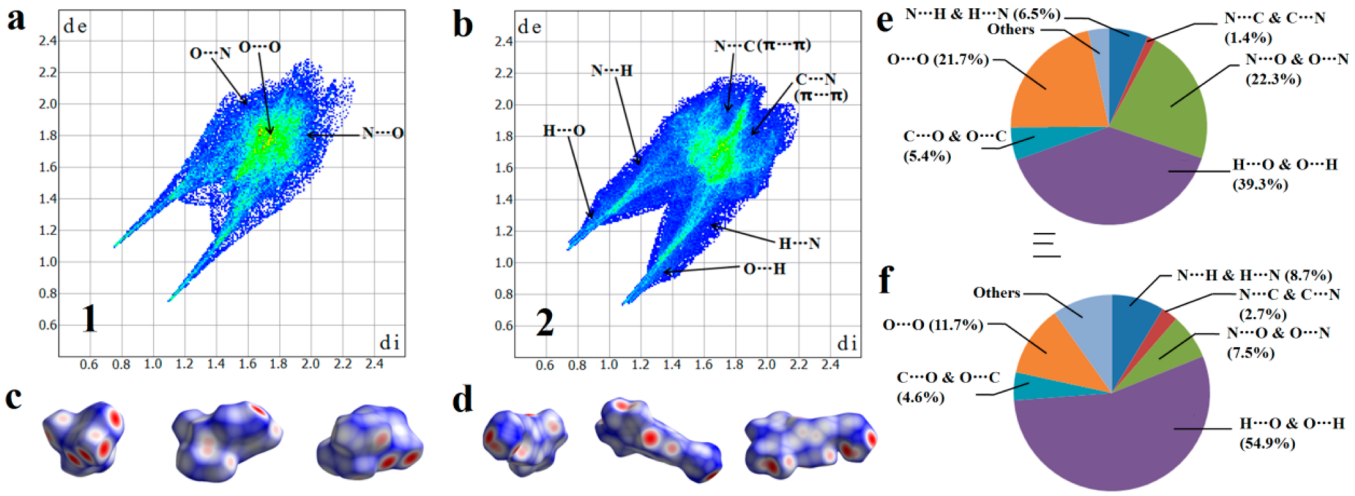

Figure 6. Two-dimensional fingerprint plots in crystal stacking for **1** and **2** as well as the associated Hirshfeld surfaces. The fingerprint plots in crystal stacking for **1** (a) and **2** (b). Images (c) and (d) showing the Hirshfeld surfaces that use color coding to represent the proximity of close contacts around **1** and **2** molecules (white, distance *d* equals the van der Waals distance; blue, *d* exceeds the van der Waals distance; red, *d* is less than van der Waals distance). In images **e** and **f**, the individual atomic contacts percentage contribution to the Hirshfeld surface are shown in the pie graphs for **1** and **2**, respectively.

Impact (IS) and friction (FS) sensitivities are also high priorities either in the manufacturing context or in military and civil energetics devices. In this work, the experimental impact and friction sensitivity values were determined for the two compounds with standard BAM drop hammer and friction tester techniques. The impact and friction sensitivities of **1** are measured to be 22 J and 240 N, respectively, which are lower than those of TNT (15 J, 353 N), RDX (7.4 J, 120 N) or HMX (7.4 J, 120 N).[13] Salt **2** is less impact and friction sensitive with an IS value of 32 J and FS value of 360 N, which classifies it as a less sensitive energetic material and further highlights its likely application potential.

Any external mechanical force acting on energetic materials can lead to a certain shape change to produce strain and store mechanical energy.[41] When this mechanical energy exceeds the limit of the energetic material, decomposition will be activated and trigger a series of explosions.[41] In order to explore the different performances of **1** and **2** on safety issues, a force field was established for both unit cells and their abilities to handle external stimuli were probed. To simplify the simulation, only vertical compression and horizontal sliding of the crystal unit cell were investigated since all direction stimuli can be split into these two types.[42] Therefore, the deformation potential (DP) can be expressed by the energy difference before and after deformation for energetic materials. For convenient comparison, the value is converted from mol units into volume units by dividing by the unit cell volume (eq 5).

$$DP = (E_{\text{after def}} - E_{\text{before def}})/V_{\text{unit cell}} \quad (5)$$

The evident differences of deformation potential between **1** and **2** are given in Figure 5. The horizontal sliding of **1** will cause the largest energy variation, while the vertical compression energy variation of **2** is only within 0–98.0 MJ m^3. Actually, the vertical compression energies of both **1** and **2** are much lower than the corresponding horizontal sliding energy which highlights the effect of face-to-face $\pi-\pi$ interactions. Taking face-to-face $\pi-\pi$ interactions as buffers, there are three buffers in the unit cell of **2** while only one buffer in **1**. For the compression simulations, these face-to-face $\pi-\pi$ interactions in **2** are able to act against external mechanical stimuli together and result in a low deformation potential. With regard to horizontal sliding, **1** and **2** are deformation restricted due to the strong and excessive intermolecular repulsion which is also revealed as red NIC isosurfaces in Figure 3. However, the flexible hydrogen bonds along two sides of the cation are also able to absorb mechanical stimuli by converting mechanical energy into intermolecular interaction energy, which elucidate the reason for the relatively lower deformation potential of **2** in the horizontal direction.

After the analysis of the unit cell, the whole crystal packing features of the energetic materials were also explored on safety issues. In this work, the 2D-fingerprint of crystals and the associated Hirshfeld surfaces were employed to show the intermolecular interactions.[43] For each point on the Hirshfeld surface, the normalized contact distance (d_{norm}) was determined by eq 6 in which d_i and d_e are measured from the surface to the nearest atom interior and nearest atom exterior to the surface interior, respectively, where r_i^{vdW} and r_e^{vdW} are the van der Waals radii of the atoms.[43] That is to say, the value of d_{norm} is negative or positive depending on the

$$d_{norm} = (d_i - d_i^{vdW})/r_i^{vdW} + (d_e - d_e^{vdW})/r_e^{vdW} \quad (6)$$

intermolecular contacts being shorter or longer than the van der Waals separations. Therefore, through the location of ($d_i d_e$) points and their relative frequencies discernible on the surface and the 2D fingerprint plot, it is possible to ascertain the distances and intensities of intermolecular interactions.

As shown in Figure 6a and 6b, a pair of remarkable spikes on bottom left (O–H, H–O, N–H and H–O interactions) in the 2D fingerprint plots of both crystals denote the hydrogen-bonds among intralayer neighboring molecules.[44] The thicker spikes of **2** indicates that more hydrogen-bonds are observed which is in agreement with our discussion. In addition, the shorter d_i+d_e of the spikes suggest stronger hydrogen-bonds. It is noteworthy that a typical pair of wings are identified as $\pi-\pi$ interactions (N–C and C–N interactions) in Figure 6b of salt **2** crystal.[44,45] By comparing the 2D fingerprint plots of eight insensitive high energetics according to US DOE standards, this index of spikes and wings can be assigned to be the important characteristic of insensitive energetic materials.[45,46] In Figures

DOI: 10.1021/ja5126275
J. Am. Chem. Soc. 2015, 137, 1697–1704

6e and 6f, the individual atomic contacts percentage contribution also confirmed the conclusion, in which O−H and N−H possess 39.3% of total weak interactions for **1** and 54.9% for **2**. For a nitrogen-containing heterocyclic ring offset, $\pi-\pi$ stacking is present as N−C and C−N interactions, while **2** provides almost twice the percentage values of **1** (2.7% vs 1.4%). Another index with regard to sensitivities is that much higher populations of O−O interactions are observed in **1** (21.7% for **1** and 11.7% for **2**). Because oxygen atoms exist mostly in nitro groups in energetic materials, additional higher relative frequencies of close O−O contacts suggests more nitro groups exposed on the molecular surfaces and increases the possibility of unexpected explosion. With respect to Hirshfeld surfaces, one judgment is that plate shapes indicate insensitivity as it represents planar conjugated molecular structures.[45] The other is that red dots (predominant intermolecular interactions) should be located on the surface edges; in this way the layers can be supported by $\pi-\pi$ stacking and thus sustain the maximum external stimuli.[44] According to these rules, the Hirshfeld surfaces of **2** (Figure 6d) fit perfectly which is again in agreement with the experimental IS and FS values where **2** is more stable than its precursor and indicate its stabilities.

CONCLUSIONS

3-Dinitromethyl-1,2,4-triazolone and its corresponding hydroxylammonium salt and have been synthesized and characterized fully. The structures of these two compounds were determined by single crystal X-ray diffraction and the ionic form shows remarkable inter- and intramolecular interactions that contribute to closer packing and thus higher density. The experimental measurements and theoretical calculations confirm that hydroxylammonium 3-dinitromethanide-1,2,4-triazolone has higher density, greater detonation performance, higher decomposition temperature, and lower impact and friction sensitivities than its parent compound which highlights its potential application as a novel energetic material. Our results suggest that designing energetic salts with π-stacking and hydrogen-bonding interactions may provide a powerful means for the development of next-generation explosives, pyrotechnics and propellants.

EXPERIMENTAL SECTION

Safety Precautions. While we have experienced no difficulties in syntheses and characterization of these materials, proper protective measures should be used. Manipulations must be carried out in a hood behind a safety shield. Face shield and leather gloves must be worn. Caution should be exercised at all times during the synthesis, characterization, and handling of any of these materials.

General Methods. Commercial analytical grade reagents were used without further purification. ^{1}H and ^{13}C spectra were recorded on a 300 MHz (Bruker AVANCE 300) nuclear magnetic resonance spectrometer operating at 300.13, and 75.48 MHz, respectively. A 500 MHz (Bruker AVANCE 500) nuclear magnetic resonance spectrometer operating at 50.69 MHz was used to obtain ^{15}N spectra for compound **2**. Chemical shifts in the ^{1}H, and ^{13}C spectra are reported relative to Me_4Si and ^{15}N NMR to $MeNO_2$. DFT and ab initio calculations were carried out using the Gaussian 09 program package.[47] The NCIs plots were calculated using Multiwfn[48] and visualized by VMD program.[49] Hirshfeld surfaces and associated 2D fingerprints were generated by CrystalExplorer 3.1.[25] The X-ray intensity data were measured on a Bruker Apex 2 CCD system equipped with a graphite monochromator and a Mo−Kα fine focus tube (λ = 0.71073 Å). An Oxford Cobra low-temperature device was used to maintain the low temperature. The melting and decomposition (onset) points were obtained on a differential scanning calorimeter (TA Instruments Co., model Q10) at a scan rate of 5 °C min^{-1}. Densities were measured at room temperature using a Micromeritics AccuPyc 1330 gas pycnometer. Impact and friction-sensitivity measurements were tested by employing a standard BAM Fallhammer and a BAM friction tester.

X-ray Crystallography. A colorless prism of dimensions 0.30 × 0.22 × 0.12 mm^3 for **1** and a yellow need-shaped crystal of dimensions 0.14 × 0.13 × 0.02 mm^3 for **2** were used for the X-ray crystallographic analysis. The X-ray intensity data were measured on a Bruker Apex 2 CCD system equipped with a graphite monochromator and a Mo−Kα fine focus tube (0.71073 Å). An Oxford Cobra low-temperature device was used to maintain the low temperature. The frames were integrated with the Bruker SAINT software package using a narrow-frame algorithm, and data were corrected for absorption effects using the multiscan method (SADABS).[50] The structures were solved and refined using the Bruker SHELXTL Software Package.[51] The synthesis and characterization are detailed in the Supporting Information.

3-Dinitromethyl-1,2,4-triazolone (1). The intermediate product 4,6-dihydroxy-5,5-dinitro-2-(dinitromethylene)-2,5-dihydropyrimidine was synthesized according to literature methods.[52] Then, 10 g of unpurified 4,6-dihydroxy-5,5-dinitro-2-(dinitromethylene)-2,5-dihydropyrimidine was added portionwise with stirring to 40 mL of 25% aqueous solution of hydrazine hydrate at 0−5 °C. The reaction mixture was stirred for another 2 h at the same temperature. The precipitate was filtered off, washed with 20 mL cold water, and dried in air to give unpurified hydrazinium 3-dinitromethanide-1,2,4-triazolone (4.5 g) which was suspended in 200 mL acetonitrile and followed by the addition of 3 mL concentrated HCl. The resulting mixture was stirred at 60 °C for 1 h. The precipitate was removed by filtration, and the filtrate was dried under vacuum to yield **1**. White solid (3.66g, 59%); ^{1}H NMR(acetone-d_6): δ11.6 (s, 1H), 8.2 (s, 1H) ppm;^{13}C NMR(acetone-d_6): δ 156.0, 135.5, 106.1 ppm; IR (KBr): ν3357, 3128, 1673, 1530, 1491, 1453, 1397, 1226, 1136, 1111, 980, 741, 717 cm^{-1}; elemental analysis, calcd (%) for $C_3H_3N_5O_5$ (189.09): C: 19.06; H: 1.60; N: 37.04; Found, C: 18.91; H: 1.61; N: 36.60.

Hydroxylammonium 3-dinitromethanide-1,2,4-triazolone (2). A solution of **1** (0.76 g, 3 mmol) in a minimum amount of acetonitrile was stirred at room temperature, while hydroxylamine (50 wt % in water, 0.21 mL, 4.2 mmol) was added. After 1 h the precipitate was filtered and air-dried to yield **2**. Yellow solid (0.84 g, 95%); ^{1}H NMR(DMSO-d_6): δ 11.4 (s, 1H), 11.1 (s, 1H), 10.0 (br, 4H) ppm;^{13}C NMR(DMSO-d_6): δ 156.2, 139.6, 124.6 ppm; ^{15}N NMR(DMSO-d_6): δ −21.9, −72.2, −112.2, −237.5, −297.9 ppm; IR (KBr): ν3153, 1740, 1697, 1595, 1485, 1323,1011, 725, 624, 586 cm^{-1}; elemental analysis, calcd (%) for $C_3H_6N_6O_6$ (222.12): C: 16.22; H: 2.72; N: 37.84; Found, C: 16.23; H: 2.68; N: 38.11.

ASSOCIATED CONTENT

Supporting Information

X-ray crystallographic files in CIF format for **1** and **2**, structure refinements, selected bond length, angles, dihedral angles, hydrogen-bonding details as well as the methodology and details for the heats of formation and other calculations. This material is available free of charge via the Internet at http://pubs.acs.org

AUTHOR INFORMATION

Corresponding Author

*jshreeve@uidaho.edu

Notes

The authors declare no competing financial interest.

ACKNOWLEDGMENTS

The authors gratefully acknowledge the support of ONR (NOOO14-12-1-0536). We are indebted to Dr. Richard J. Staples for considerable assistance with crystal structuring and Dr. Xiujuan Qi and Dr. Tian Lu for calculations.

DOI: 10.1021/ja5126275
J. Am. Chem. Soc. 2015, 137, 1697−1704

REFERENCES

(1) Agrawal, J. P.; Hodgson, R. D. *Organic Chemistry of Explosives*; Wiley: New York, 2007.
(2) Gao, H.; Shreeve, J. M. *Chem. Rev.* **2011**, *111*, 7377−7436.
(3) Brinck, T. *Green Energetic Materials*; Wiley: New York, 2014.
(4) Giles, J. *Nature* **2004**, *427*, 580−581.
(5) Huynh, M. H. V.; Coburn, M. D.; Meyer, T. J.; Wetzler, M. *Proc. Natl. Acad. Sci. U.S.A.* **2006**, *103*, 10322−10327.
(6) Huynh, M. H. V.; Hiskey, M. A.; Meyer, T. J.; Wetzler, M. *Proc. Natl. Acad. Sci. U.S.A.* **2006**, *103*, 5409−5412.
(7) Thottempudi, V.; Gao, H.; Shreeve, J. M. *J. Am. Chem. Soc.* **2011**, *133*, 6464−6470.
(8) Göbel, M.; Tchitchanov, B. H.; Murray, J. S.; Politzer, P.; Klapötke, T. M. *Nat. Chem.* **2009**, *1*, 229−235.
(9) Thundat, T. *Nat. Nanotechnol.* **2008**, *3*, 133−134.
(10) Bolton, O.; Matzger, A. J. *Angew. Chem., Int. Ed.* **2011**, *50*, 8960−8963.
(11) Landenberger, K. B.; Bolton, O.; Matzger, A. J. *Angew. Chem., Int. Ed.* **2013**, *52*, 6468−6471.
(12) Li, S.; Wang, Y.; Qi, C.; Zhao, X.; Zhang, J.; Zhang, S.; Pang, S. *Angew. Chem., Int. Ed.* **2013**, *52*, 14031−14035.
(13) Zhang, J.; Shreeve, J. M. *J. Am. Chem. Soc.* **2014**, *136*, 4437−4445.
(14) Armand, M.; Endres, F.; MacFarlane, D. R.; Ohno, H.; Scrosati, B. *Nat. Mater.* **2009**, *8*, 621−629.
(15) Zhang, J.; Parrish, D. A.; Shreeve, J. M. *Chem.—Asian J.* **2014**, *9*, 2953−2960.
(16) Fischer, N.; Fischer, D.; Klapötke, T. M.; Piercey, D. G.; Stierstorfer, J. *J. Mater. Chem.* **2012**, *22*, 20418−20422.
(17) Singh, R. P.; Verma, R. D.; Meshri, D. T.; Shreeve, J. M. *Angew. Chem., Int. Ed.* **2006**, *45*, 3584−3601.
(18) Dippold, A. A.; Klapötke, T. M. *J. Am. Chem. Soc.* **2013**, *135*, 9931−9938.
(19) Witze, A. *Nature* **2013**, *500*, 509−510.
(20) Pérez, J.; Riera, L. *Chem. Commun.* **2008**, *5*, 533−543.
(21) Faul, C. F.; Antonietti, M. *Adv. Mater.* **2003**, *15*, 673−683.
(22) Nelyubina, Y. V.; Antipin, M. Y. E.; Lyssenko, K. A. *Russ. Chem. Rev.* **2010**, *79*, 167−187.
(23) Turner, D. R.; Edwards, A. J.; Piltz, R. O. *CrystEngComm* **2012**, *14*, 6447−6451.
(24) Astrat'ev, A.; Dashko, D.; Stepanov, A. Proceedings of the New Trends in Research of Energetic Materials, Pardubice, Czech Republic, April 9−11, 2014; University of Pardubice: Pardubice, Czech Republic, 2014; pp 469−481.
(25) Wolff, S. K.; Grimwood, D. J.; McKinnon, J. J.; Turner, M. J.; Jayatilaka, D.; Spackman, M. A. *CrystalExplorer*, version 3.1; University of Western Australia: Crawley, Australia, 2012.
(26) Zhang, C.; Kang, B.; Cao, X.; Xiang, B. *J. Mol. Model.* **2010**, *18*, 2247−2256.
(27) Molčanov, K.; Sabljić, I.; Kojić-Prodić, B. *CrystEngComm* **2011**, *13*, 4211−4217.
(28) Jose, D.; Datta, A. *Cryst. Growth. Des.* **2011**, *11*, 3137−3140.
(29) Allen, F. H. *Acta Crystallogr., Sect. B* **2002**, *58*, 380−388.
(30) Klapötke, T. M.; Piercey, D. G.; Stierstorfer, J. *Chem.—Eur. J.* **2011**, *17*, 13068−13077.
(31) Johnson, E. R.; Keinan, S.; Mori-Sanchez, P.; Contreras-Garcia, J.; Cohen, A. J.; Yang, W. *J. Am. Chem. Soc.* **2010**, *132*, 6498−6506.
(32) Grimme, S.; Ehrlich, S.; Goerigk, L. *J. Comput. Chem.* **2011**, *32*, 1456−1465.
(33) Neese, F. *WIREs Comput. Mol. Sci.* **2012**, *2*, 73−78.
(34) Parr, R. G.; Yang, W. *Density Functional Theory of Atoms and Molecules*; Oxford University Press: Oxford, U.K., 1989.
(35) Curtiss, L. A.; Raghavachari, K.; Trucks, G. W.; Pople, J. A. *J. Chem. Phys.* **1991**, *94*, 221−7230.
(36) Westwell, M. S.; Searle, M. S.; Wales, D. J.; Williams, D. H. *J. Am. Chem. Soc.* **1995**, *117*, 5013−5015.
(37) Jenkins, H. D. B.; Tudela, D.; Glasser, L. *Inorg. Chem.* **2002**, *41*, 2364−2367.
(38) Sućeska, M. *EXPLO5 6.01*; Brodarski Institute: Zagreb, Croatia, 2013.
(39) Yu, Z.; Bernstein, E. R. *J. Phys. Chem. A* **2013**, *117*, 1756−1764.
(40) Zhang, J. Y.; Du, H. C.; Wang, F.; Gong, X. D.; Huang, Y. S. *J. Phys. Chem. A* **2011**, *115*, 6617−6621.
(41) Zhang, C. *J. Phys. Chem. B* **2007**, *111*, 14295−14298.
(42) Zhang, C.; Wang, X.; Huang, H. *J. Am. Chem. Soc.* **2008**, *130*, 8359−8365.
(43) Spackman, M. A.; Jayatilaka, D. *CrystEngComm* **2009**, *11*, 19−32.
(44) Zhang, C.; Xue, X.; Cao, Y.; Zhou, Y.; Li, H.; Zhou, J.; Gao, T. *CrystEngComm* **2013**, *15*, 6837−6844.
(45) Ma, Y.; Zhang, A.; Zhang, C.; Jiang, D.; Zhu, Y.; Zhang, C. *Cryst. Growth. Des.* **2014**, *14*, 4703−4713.
(46) Manual, D. O. E. *DOE Explosives Safety Manual* **2006**, *440*, 1−1A.
(47) Frisch, M. J.; Trucks, G. W.; Schlegel, H. G.; Scuseria, G. E.; Robb, M. A.; Montgomery, J. A., Jr; Vreven, T.; Kudin, K. N.; Burant, J. C.; Millam, J. M.; Iyengar, S. S.; Tomasi, J.; Barone, V.; Mennucci, B.; Cossi, M.; Scalmani, G.; Rega, N.; Petersson, G. A.; Nakatsuji, H.; Hada, M.; Ehara, M.; Toyota, K.; Fukuda, R.; Hasegawa, J.; Ishida, M.; Nakajima, T.; Honda, Y.; Kitao, O.; Nakai, H.; Klene, M.; Li, X.; Knox, J. E.; Hratchian, H. P.; Cross, J. B.; Bakken, V.; Adamo, C.; Jaramillo, J.; Gomperts, R.; Stratmann, R. E.; Yazyev, O.; Austin, A. J.; Cammi, R.; Pomelli, C.; Ochterski, J. W.; Ayala, P. Y.; Morokuma, K.; Voth, G. A.; Salvador, P.; Dannenberg, J. J.; Zakrzewski, V. G.; Dapprich, S.; Daniels, A. D.; Strain, M. C.; Farkas, O.; Malick, D. K.; Rabuck, A. D.; Raghavachari, K.; Foresman, J. B.; Ortiz, J. V.; Cui, Q.; Baboul, A. G.; Clifford, S.; Cioslowski, J.; Stefanov, B. B.; Liu, A. L. G.; Piskorz, P.; Komaromi, I.; Martin, R. L.; Fox, D. J.; Keith, T.; Al-Laham, M. A.; Peng, C.; Nanayakkara, A.; Challacombe, M.; Gill, P. M. W.; Johnson, B.; Chen, W.; Wong, M.; Gonzalez, C.; Pople, J. A. *Gaussian 03*, revision D.01; Gaussian, Inc.: Wallingford, CT, 2004.
(48) Lu, T.; Chen, F. J. *J. Comput. Chem.* **2012**, *33*, 580−592.
(49) Humphrey, W.; Dalke, A.; Schulten, K. *J. Mol. Graphics Modell.* **1996**, *14*, 33−38.
(50) *Bruker SAINT (SADABS)*, v2008/1; Bruker AXS Inc.: Madison, Wisconsin, 2008.
(51) *Bruker SHELXTL*, v2008/1; Bruker AXS Inc.: Madison, Wisconsin, 2008.
(52) Astrat'ev, A. A.; Dashko, D. V.; Mershin, A. Y.; Stepanov, A. I.; Urazgil'deev, N. A. *Russ. J. Org. Chem.* **2001**, *37*, 729−733.

DOI: 10.1021/ja5126275
J. Am. Chem. Soc. 2015, 137, 1697−1704